Effect of powder atomising route on the surface quality and mechanical performance of AISI 316L samples produced via laser powder bed fusion process

Available online at www.sciencedirect.com

ScienceDirect

Procedia CIRP 118 (2023) 688–693

www.elsevier.com/locate/procedia

16th CIRP Conference on Intelligent Computation in Manufacturing Engineering, CIRP ICME '22, Italy

Effect of powder atomising route on the surface quality and mechanical performance of AISI 316L samples produced via laser powder bed fusion process

Erika Lannunziata[a], Niccolò Zapparoli[b], Luca Iuliano[a], Abdollah Saboori [a,*]

[a]*Integrated Additive Manufacturing Center (IAM), Department of Management and Production Engineering (DIGEP), , Politecnico di Torino, Corso Duca Degli Abruzzi, 24, 10129, Torino, Italy*

[b]*Department of Applied Science and Technology, Politecnico Di Torino, Corso Duca degli Abruzzi 24, 10129 Torino, Italy*

* Corresponding author. Tel.: +39-0110907285; E-mail address: abdollah.saboori@polito.it,

Abstract

Laser powder bed fusion (LPBF) is an additive manufacturing technology that allows the production of the component with complex geometry and excellent mechanical properties. So far, many process variables have been investigated to control the process and reach the best quality. One of the key factors that may affect the quality of the parts produced by the LPBF process is the type of powder that is the goal of this research. The work starts with producing two sets of cubic samples with different process parameters. The first set uses GA powder as feedstock material, while the second uses WA powder. The as-built parts are then characterised in terms of density and surface roughness. After selecting the optimal set of process parameters, tensile samples are produced and tested.

Keywords: Additive manufacturing; Surface mechanical treatment; 316L stainless steel; Selective laser melting; Residual stress.

1. Introduction

The laser powder bed fusion (L-PBF) process is an additive manufacturing (AM) technique that builds a component by melting and solidifying powdered feedstock using a laser as an energy source. It is well documented that many factors in this process can influence the quality of the as-built components [1,2]. Several studies looked into optimising process parameters to achieve the highest achievable density. Laser power, scanning speed, hatch spacing, and layer thickness are the most commonly considered parameters for optimisation [3,4]. However, the aforementioned parameters can be combined into a single value termed volumetric energy density (VED), which is calculated as follow:

$$VED[\frac{J}{mm^3}] = \frac{P}{z \cdot h \cdot v_s} \quad (1)$$

As a matter of fact, VED is related to the amount of volumetric unit energy supplied to the powder bed [5]. It is reported that too high VED results in overheating, while too low one promotes defect formation [6]. However, it should be underlined that if the same VED value is used with a different set of parameters, the results can be quite different [7]. However, the feedstock material, which affects the as-built mechanical properties and microstructure, is a key factor that has received little attention in the literature [8,9]. In fact, the behaviour of metallic powder particles depends on the atomisation process that defines the shape and particle size distribution of the powder. Gas-atomised powders (GA) are well-known for having a quasi-spherical shape, whereas water-atomised ones (WA) have an irregular shape [10]. Therefore, GA powders with a semi-spherical shape expected to ensure a good flowability are widely used in the metal AM sector. Cacace et al. studied the influence of two parameters (layer thickness and scan speed) on the density of AISI 316L cubes

10.1016/j.procir.2023.06.118

using WA and GA powders [11]. Furthermore, Li et al. investigated the densification mechanism of 316L GA and WA powders during the L-PBF process [12]. However, the WA powder has not been considered an option in the literature; as a result, the process parameters have not been optimised, and the outcome properties have not been thoroughly evaluated. Hence, this study studied deeply the quality of the as-built L-BPF AISI 316L samples using the GA and WA powders as the feedstock material. For this reason, this study focuses on mechanical properties and surface roughness, as well as how the feedstock material influences these features. The initial stage was to optimise process parameters to maximise the density of specimens. Then, tensile samples were built to analyse the effect of the type of powder on the mechanical performance of the AISI 316L samples produced using the L-PBF process.

2. Materials and methods

The experimental process consisted of different steps. The first step was the production of cubic samples, which assessed their relative density and surface roughness. Subsequently, some tensile samples were produced and then tested to study the tensile properties. The material used in this work was the AISI 316L, austenitic stainless steel, which attracted interest for its excellent corrosion resistance combined with good mechanical properties. In particular, in this study, two feedstock materials were compared, one was the GA powder supplied by EOS, and one was the WA powder by Pometon. The chemical composition is reported in Table 1. Both types of powder had a size range of 15 –50 μm. Before loading feedstock material into the machine, the raw material was dried in an oven for one hour at 80°C.

Table 1. Chemical composition of the starting powders used in this work.

Element	Cr	Ni	Mo	C	N	Fe
GA	17-19	13-15	2.2-3	0.03	0.1	Balance
WA	16.5-18.5	10-13	2-2.5	<0.03	<0.11	Balance

2.1. Design of experiments

The first purpose of this project was to find the best parameters for maximising density. The sample production in this work was performed using a Concept laser Mlab Cusing R. 32 cubic samples with a nominal dimension of 12×12×12 mm3 were produced following a design of experiment approach. The first job was built with GA powder, while the second with the WA one using the same process parameters. Table 2 shows the parameters window used, particularly four scanning speeds (Ss) of 500, 600, 700, and 800 mm/s, and five hatch spacing (Hs) of 64, 74, 84, 94, and 104 μm. Moreover, the layer thickness (Lt) was kept constant at 25 μm, and the laser power (Lp) was set at 95 W. Furthermore, in Table 2, the VED was computed according to equation (1), which varied in the range of 56.5 and 99.0 J/mm^3. Samples from numbers 1 to 8 were printed with the same process parameters as 9 to 16. They differed in their scanning strategy: in the first half of the samples (1-8), the laser path followed a chessboard pattern, as shown in Figure 1a. In the second half (9-16), the scanning strategy was stripe with a rotation between each successive layer of 67°, shown in Figure 1b. Specifically, Figure 1 illustrates a schematic of the top surface on the left and the real top surface on the right.

Table 2. Process parameters used in this work.

Samples	Scanning speed [mm/s]	Hatch distance [mm]	VED [J/mm^3]
1/9	500	0.084	90.5
2/10	600	0.084	75.4
3/11	700	0.084	64.6
4/12	800	0.084	56.5
5/13	600	0.064	99.0
6/14	600	0.074	85.6
7/15	600	0.094	67.4
8/16	600	0.104	60.9

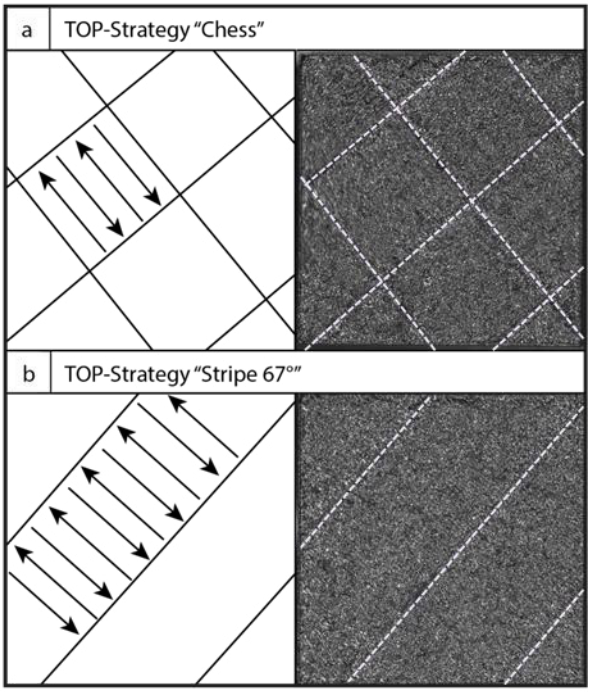

Fig. 1. (a) Chess/meander scanning strategy illustration; (b) Stripe/67 scanning strategy. The arrows in the sketch show the filling laser path.

The density of samples was evaluated using an Archimedes balance using distilled water at 25°C following the Archimedes principles [13].

The relative density of 316L samples was calculated using 7.98 g/cm^3 as the theoretical value. Following the statistical approach, the measurements were repeated three times per sample, and their average was reported as the relative density. Subsequently, the surface roughness measurement was performed with a profilometer RTP 80. Finally, the tensile specimens were produced with the most promising parameters, and the tensile test was performed at room temperature setting the strain speed constant at 2 mm/min.

3. Results and discussion

3.1 *Density*

Figure 2 illustrates the variation of the relative density of all the as-built samples as a function of VED. Although the GA and WA samples were built with the same process parameters,

it is evident that using the GA powder resulted in higher densities than those produced using the WA ones. As can be seen, a maximum density of 99.8% was achieved in the sample GA14, which corresponded to the Stripe/67 scanning strategy with a scanning speed of 600 mm/s and a hatch spacing of 0.084 mm. However, it is found that using the same parameters does not essentially result in the highest density for the samples produced using the WA powder. As a result, the outcome of process parameter optimisation for both powders were not identical. Despite this, using the Stripe/67 scanning method, a scanning speed of 500mm/s, and a hatch spacing at 0.084 mm, the WA09 sample achieved a density of over 99 %. Moreover, the collected density data agree with the different densification behaviour reported in the literature [14]. Previous studies pointed out that the density can be influenced by the chemical composition and shape of the powder. It is well documented that the chemical composition of the water atomised powders is affected by a larger oxygen content than the gas atomised one. As reported by Li et al., the oxidation of particles could worsen the wettability-[12]. Indeed, the molten pool did not easily wet the oxidation-coated surface, so a porous melted layer would be formed. In addition, the GA powder is characterised by a spherical shape, whereas the WA one has an irregular shape. As a result, GA has better flowability and higher packing density, and so using this powder led to obtaining higher densification.

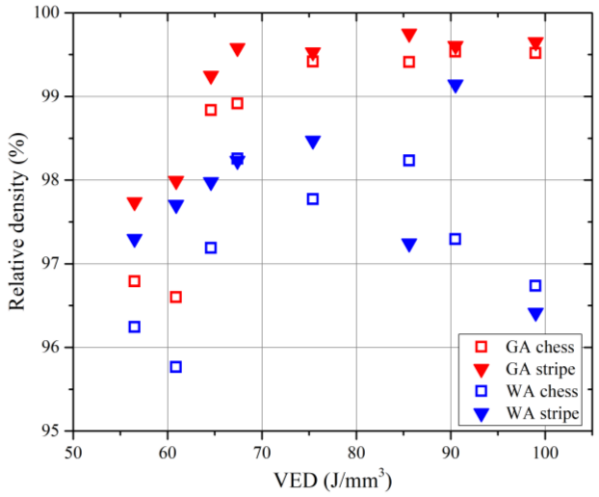

Fig. 2. Relative density for all samples produced as a function of VED. The arrows show the densest sample for each type of feedstock material.

Beyond the feedstock impact on the density, VED fluctuation can also affect the porosity formation. Indeed, Figure 3 shows the outcomes highlighting the difference between GA and WA samples with blue and red markers and Chess/Meander and Stripe/67 scanning strategy with squares and triangles, respectively. The GA samples exhibited an increase of relative density in the range of 65-70 J/mm^3, reaching an almost steady region where density remained constant as VED increased, as confirmed in literature [15]. However, the trend of the WA samples was significantly different. Precisely, at lower VED, density grew similar to the case of GA samples, but at higher VED, it dropped. In addition, the scanning strategy influence was remarkable, as the Stripe/67 strategy provided samples with a higher density in the majority of cases.

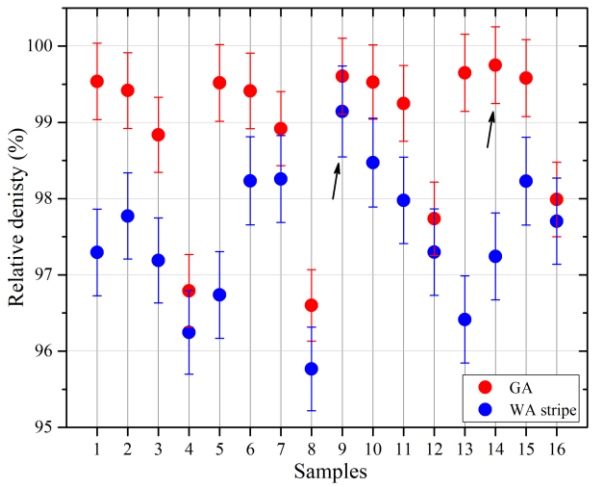

Fig. 3. Relative density of all the AISI 316L samples; red dots are for GA and blue dots are for WA powder.

Figure 4 shows how scanning speed and hatch spacing can affect part density in different ways.

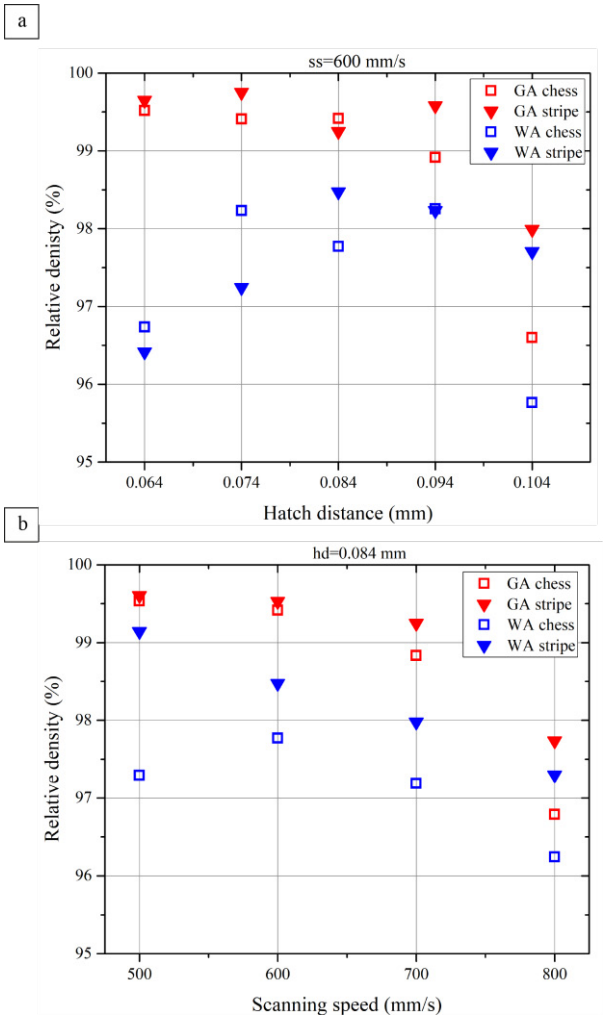

Fig. 4. Relative density as a function of (a) scanning speed; and (b) hatch spacing.

In particular, Figure 4.a shows the scan speed effect on the density keeping the hatch distance constant at 0.084 mm. The density decreased as the speed increased, especially for the WA samples. Indeed, low speed could balance the low flowability and packing density of WA powders; thereby, with WA powders, high productivity could not be suitable for full dense components. Conversely, Figure 4.b points out the effect of hatch distance setting the speed at 600 mm/s. The samples built with GA powder exhibited a density of over 99%, raising the hatch spacing to 0.094 mm, where it fell down. This behaviour occurred when the overlap between tracks was insufficient, whereby the laser could not succeed to melti these regions. The WA density reached a maximum setting the hatch distance between 0.084 mm to 0.094 mm, even though extending or reducing the hatch spacing from this range resulted in density dropping. The density is the leading property in choosing the parameters for producing tensile samples. Although, as previously stated, two different sets of process parameters maximised the density for GA and WA powder. Nevertheless, the tensile samples were produced with the set of process parameters that optimised the density of GA samples aiming to compare properties with the same process parameters. For the building of tensile samples, the GA14 parameters were adopted, namely the Stripe/67 as scanning strategy, 600 mm/s and 74 µm as speed and hatch distance, respectively.

2.2. Surface roughness

The top surface roughness as a function of VED is shown in Figure 5.a. The samples produced with GA powder generally had a lower surface roughness when compared with samples produced with WA powder. Regarding GA samples, the surface roughness trend was similar to the relative density one. Indeed the GA samples showed a decrease in surface roughness in the range of 70-75 J/mm^3. Meanwhile, from 85 J/mm^3, the roughness raised slightly.

Nonetheless, the WA trend behaviour was opposite to the GA one. At lower VED, the two types of powder resulted in the almost same surface roughness. However, the GA samples enhanced the surface smoothness at higher VED, while WA samples increased their surface roughness. According to the results, it would not be possible to achieve the lowest possible surface roughness for both WA and GA powders using the same set of process parameters. Therefore, the lowest top surface roughness of 7.89 µm was achieved by GA6 (VED=85.6 J/mm^3), and among the WA samples, WA12 (VED=56.5 J/mm^3) reached 10.59 µm.

The surface roughness was also measured on the lateral surfaces, and the results are collected in Figure 5.b. In this case, both GA and WA samples showed the same trend as a function of VED, and the surface roughness slightly decreased as VED increased. In addition, the WA samples had lower surface roughness than the GA samples.

The difference in surface roughness between lateral and top surfaces is a well-known phenomenon in literature [16]. The surface roughness appears to be lower on the top surface and higher on the lateral surfaces. Conversely, Figures 5-6 reported that the lateral surfaces were smoother than the top ones. In particular, for the best process conditions (GA14), figure 6 shows the roughness profile where the blue line (the lateral surface) has lower and tighter peaks than the red line (top surface).

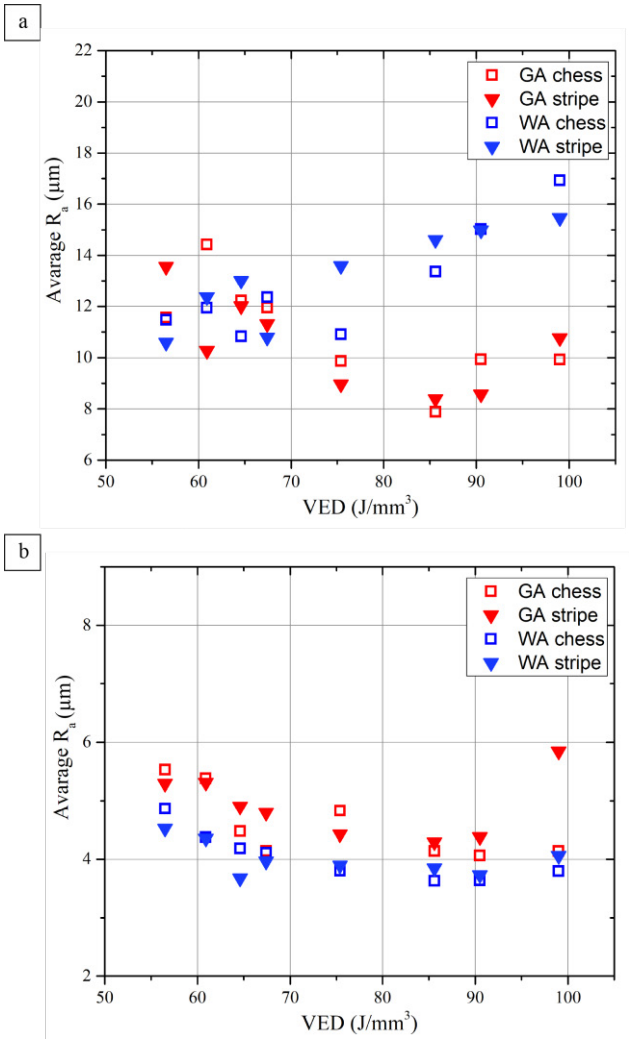

Fig. 5. Surface roughness as a function of VED for (a) top surface; and (b) lateral surface.

The feedstock material is not the only parameter that can affect the surface roughness in the L-PBF process. Indeed, as seen before, also VED influences the surface quality of the as-built samples. During the production of the samples, two parameters were varied, scanning speed and hatch spacing, and both influenced the surface roughness. According to state of the art, hatch distance is the parameter that most influences surface finishing. For AISI 316L, decreasing hatch spacing reduces surface roughness until an optimum level, where further reductions are detrimental [17]. As shown in Figure 7.a, the effect of hatch spacing was similar on two types of feedstock material. However, WA samples reached the lowest surface roughness at 0.094 mm while GA samples at 0.074 mm. Scanning speed had an inverse relationship with surface roughness. Especially when scan speed grows too high to fully melt the powder bed surface, it might have a negative impact on surface quality [16].

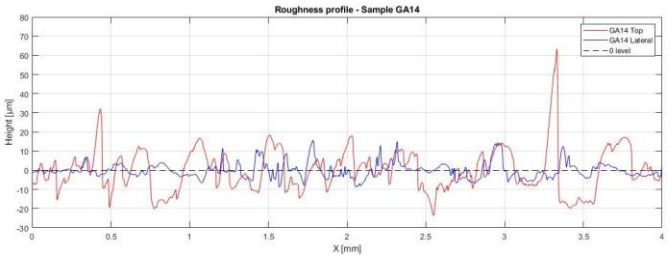

Fig. 6. Roughness profile of the top surface (red) and the lateral one (blue) of the GA14 sample.

2.3. Mechanical properties

As already reported, the optimised process parameters used to produce tensile samples were those associated with the samples with the maximum density. The tensile samples produced were 8: five with GA powder and 3 with WA one. The samples were produced horizontally on the building platform.

Table 3 summarises the tensile test outputs. Comparing the yield strength (YS) of the sample, it is revealed that the GA samples almost reached 540 MPa (sample 3), whereas the minimum YS value was around 505 MPa (sample 5). The yield strength obtained for 316L samples produced using GA powder was confirmed in the literature by Liu et al. [12]. On the other hand, the WA samples did not attain such YS limits and fell between 460 and 480 MPa. Moreover, the ultimate tensile strength (UTS) reached the mean values found in the literature, and the WA samples achieved lower values than the GA samples, as in the case of the YS. As can be seen in Figure 8, the different feedstock materials also influenced the elongation of the samples.

Table 3. Mechanical test results. Yield strength (YS), ultimate tensile strength (UTS), elongation at maximum stress (ε), elongation at failure (ε_f).

Sample	YS [MPa]	UTS [MPa]	ε [%]	ε_f [%]
GA01	522.9	617.6	17.76	24.34
GA02	516.2	611.4	17.08	24.83
GA03	539.5	614.9	18.38	25.49
GA04	517.6	608.6	18.81	27.03
GA05	506.2	599.8	18.74	25.82
WA01	464.6	576.5	21.15	22.63
WA02	480.2	596.0	18.20	19.57
WA03	464.4	573.3	19.31	20.16

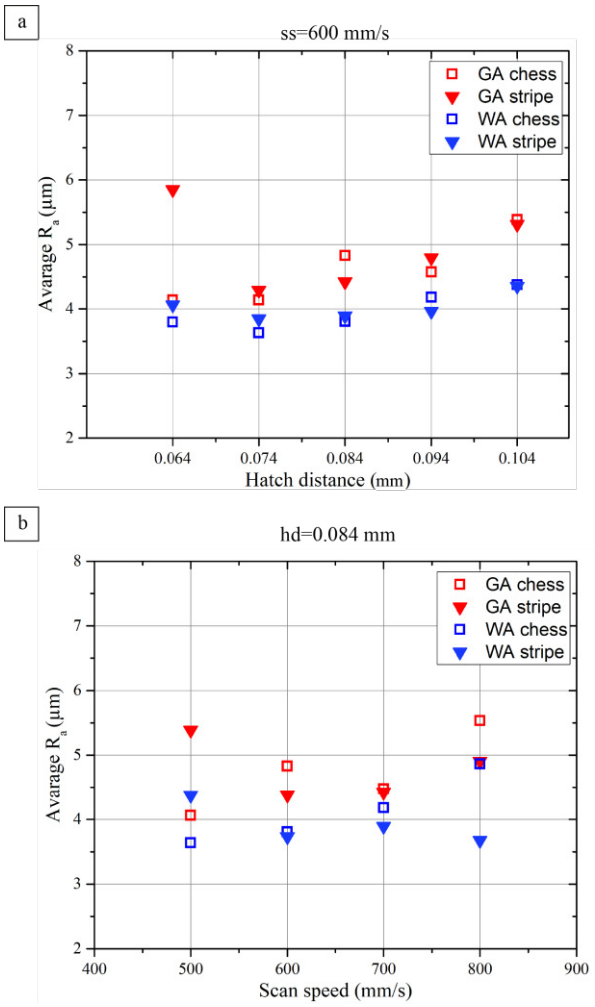

Fig. 7. Surface roughness as a function of (a) hatch spacing, and (b) scanning speed.

Indeed, the GA samples had a lower elongation (ε) than the WA samples, but the latter had a short necking zone where the elongation continued for less than 2%. On the other hand, GA samples continued to deform for more than 6% longer than the WA ones, resulting in a higher elongation at failure.

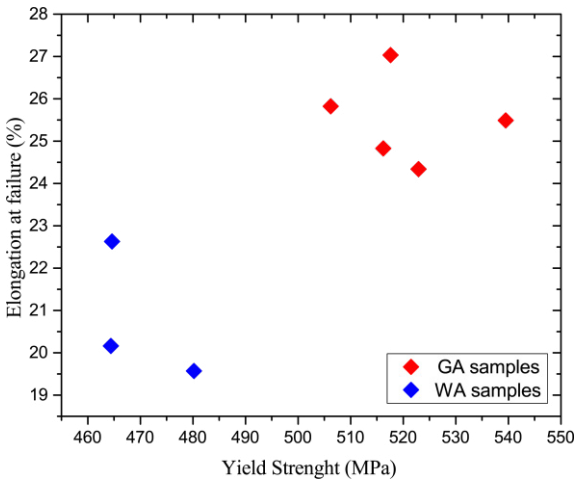

Fig. 8. Elongation at failure as function of yield strength.

4. Conclusions

In this work, the effect of the powder atomization route on the densification, roughness and mechanical properties of AISI 316L samples produced via the L-PBF process is studied. By analysing all the findings in this research, the following conclusion can be drawn as follow:

- Regarding the density results, the density of gas atomised samples was normally higher due to the lower oxygen content and higher flowability.
- The WA and GA samples were built with an identical DOE, although the maximum density was achieved at different combinations of process parameters.
- In both examples of feedstock material, increasing VED resulted in increased densification; however, after reaching a threshold value, the density of WA samples began to decline.
- The surface roughness showed two different trends and values when considering the top and lateral surfaces; the latter has a smoother surface.
- Considering only the top surfaces, the roughness was comparable between the two types of feedstock material at lower VED. However, increasing the energy provided to the melt pool, the surface of GA samples decreased in roughness, while the WA one increased.
- In terms of mechanical qualities, the GA powder enabled the creation of samples with higher YS and elongation at failure. Indeed, when GA samples attained ultimate, specimens continued to deform, whereas the WA samples failed at a lower elongation.

References

[1] M.H. Mosallanejad, B. Niroumand, A. Aversa, D. Manfredi, A. Saboori, Laser Powder Bed Fusion in-situ alloying of Ti-5%Cu alloy: Process-structure relationships, J. Alloys Compd. (2020) 157558. https://doi.org/https://doi.org/10.1016/j.jallcom.2020.157558.

[2] R. Barros, F.J.G. Silva, R.M. Gouveia, A. Saboori, G. Marchese, S. Biamino, A. Salmi, E. Atzeni, Laser powder bed fusion of inconel 718: Residual stress analysis before and after heat treatment, Metals (Basel). 9 (2019). https://doi.org/10.3390/met9121290.

[3] M. Dadkhah, M.H. Mosallanejad, L. Iuliano, A. Saboori, A Comprehensive Overview on the Latest Progress in the Additive Manufacturing of Metal Matrix Composites: Potential, Challenges, and Feasible Solutions, Acta Metall. Sin. (English Lett. 34 (2021) 1173–1200. https://doi.org/10.1007/s40195-021-01249-7.

[4] S. Greco, K. Gutzeit, H. Hotz, B. Kirsch, J.C. Aurich, Selective laser melting (SLM) of AISI 316L—impact of laser power, layer thickness, and hatch spacing on roughness, density, and microhardness at constant input energy density, Int. J. Adv. Manuf. Technol. 108 (2020) 1551–1562. https://doi.org/10.1007/s00170-020-05510-8.

[5] M. Aristizabal, P. Jamshidi, A. Saboori, S.C. Cox, M.M. Attallah, Laser powder bed fusion of a Zr-alloy: Tensile properties and biocompatibility, Mater. Lett. 259 (2020) 126897. https://doi.org/https://doi.org/10.1016/j.matlet.2019.126897.

[6] M.H. Mosallanejad, B. Niroumand, A. Aversa, A. Saboori, In-situ alloying in laser-based additive manufacturing processes: A critical review, J. Alloys Compd. 872 (2021) 159567. https://doi.org/https://doi.org/10.1016/j.jallcom.2021.159567.

[7] M.H. Mosallanejad, S. Sanaei, M. Atapour, B. Niroumand, L. Iuliano, A. Saboori, Microstructure and Corrosion Properties of CP-Ti Processed by Laser Powder Bed Fusion under Similar Energy Densities, Acta Metall. Sin. (English Lett. (2022). https://doi.org/10.1007/s40195-022-01376-9.

[8] A. Aversa, A. Saboori, G. Marchese, L. Iuliano, M. Lombardi, P. Fino, Recent Progress in Beam-Based Metal Additive Manufacturing from a Materials Perspective: A Review of Patents, J. Mater. Eng. Perform. 30 (2021) 8689–8699. https://doi.org/10.1007/s11665-021-06273-3.

[9] A. Saboori, A. Aversa, F. Bosio, E. Bassini, E. Librera, M. De Chirico, S. Biamino, D. Ugues, P. Fino, M. Lombardi, An investigation on the effect of powder recycling on the microstructure and mechanical properties of AISI 316L produced by Directed Energy Deposition, Mater. Sci. Eng. A. (2019) 138360. https://doi.org/https://doi.org/10.1016/j.msea.2019.138360.

[10] W. Chen, G. Yin, Z. Feng, X. Liao, Effect of powder feedstock on microstructure and mechanical properties of the 316L stainless steel fabricated by selective laser melting, Metals (Basel). 8 (2018). https://doi.org/10.3390/met8090729.

[11] S. Cacacea, A.G. Demir, Q. Semeraroa, Densification mechanism for different types of stainless steel powders in Selective Laser Melting, in: 10th CIRP Conf. Intell. Comput. Manuf. Eng. - CIRP ICME '16, 2017: pp. 475–480.

[12] R. Li, Y. Shi, Z. Wang, L. Wang, J. Liu, W. Jiang, Densification behavior of gas and water atomized 316L stainless steel powder during selective laser melting, Appl. Surf. Sci. 256 (2010) 4350–4356. https://doi.org/10.1016/j.apsusc.2010.02.030.

[13] M. Galati, S. Defanti, A. Saboori, G. Rizza, E. Tognoli, N. Vincenzi, A. Gatto, L. Iuliano, An investigation on the processing conditions of Ti-6Al-2Sn-4Zr-2Mo by electron beam powder bed fusion: Microstructure, defect distribution, mechanical properties and dimensional accuracy, Addit. Manuf. 50 (2022) 102564. https://doi.org/https://doi.org/10.1016/j.addma.2021.102564.

[14] S. Hoeges, A. Zwiren, C. Schade, Additive manufacturing using water atomized steel powders, Met. Powder Rep. 72 (2017) 111–117. https://doi.org/10.1016/j.mprp.2017.01.004.

[15] A. Leicht, M. Fischer, U. Klement, L. Nyborg, E. Hryha, Increasing the Productivity of Laser Powder Bed Fusion for Stainless Steel 316L through Increased Layer Thickness, J. Mater. Eng. Perform. 30 (2021) 575–584. https://doi.org/10.1007/s11665-020-05334-3.

[16] K. Mumtaz, N. Hopkinson, Top surface and side roughness of Inconel 625 parts processed using selective laser melting, Rapid Prototyp. J. 15 (2009) 96–103. https://doi.org/10.1108/13552540910943397.

[17] M. Badrossamay, E. Yasa, J. Van Vaerenbergh, J.-P. Kruth, Improving Productivity Rate in SLM of Commercial Steel Powders, in: Tech. Pap. - Soc. Manuf. Eng., 2009: pp. 1–13. Article.

.